RSC Advances

PAPER

View Article Online
View Journal | View Issue

Cite this: *RSC Adv.*, 2019, **9**, 39163

Nonfullerene acceptors comprising a naphthalene core for high efficiency organic solar cells†

Zhe Zhang,[a] Xinyue Cui,[ab] Miao Li,[b] Yahui Liu,*[b] Dawei Li,[a] Pengcheng Jiang[b] and Zhishan Bo*[b]

Received 6th October 2019
Accepted 21st November 2019

DOI: 10.1039/c9ra08092a

rsc.li/rsc-advances

A fused-ring electron acceptor (FREA) NDIC is designed and synthesized. Inspired by IDIC, NDIC was constructed by replacing the benzene with a naphthalene ring in its core unit. IDIC exhibits an optical bandgap of 1.60 eV and a lower lowest unoccupied molecular orbital (LUMO) energy level of −3.92 eV. In comparison, NDIC displays an optical band gap of 1.72 eV and a higher lying LUMO energy level of −3.88 eV. Due to the higher energy level, inverted devices based on NDIC exhibit a higher open circuit voltage (V_{oc}) of 0.90 V, which is much higher than that of IDIC (0.77 V). After a series of optimizations, a power conversion efficiency (PCE) of 9.43% was obtained with a PBDB-T:NDIC blend active layer, in comparison, a PCE of 9.19% was achieved based on IDIC. Our results demonstrate that a tiny variation in the molecular structure could dramatically affect the optical and electrochemical properties, and thus the photovoltaic performance.

1. Introduction

Polymer solar cells (PSCs) as clean energy conversion devices have received extensive attention due to their light weight, low cost, flexibility, and suitability for roll-to-roll printing.[1–5] In the past several decades, the active layer of PSC devices, typically with a bulk heterojunction (BHJ) structure, usually consists of conjugated polymers as donors and fullerene derivatives as acceptors. The power conversion efficiency (PCE) has reached over 11% for PSCs based on fullerene derivative acceptors. However, it is hard to further enhance the PCE of fullerene based PSCs due to the inherent limitations of fullerene derivatives, such as low absorption coefficient and limited absorption region.[6] To further enhance the photovoltaic performance of PSCs, fused-ring electron acceptors (FREAs) were developed to fabricate high efficiency PSCs.[7–9] Compared with traditional fullerene acceptors, nonfullerene acceptors have many advantages, such as facile synthesis, high absorption coefficient, adjustable energy levels, wide absorption region and so on.[10,11] A series of high efficiency nonfullerene acceptors (NFAs) with an electron donating ladder-type central core and two electron withdrawing end groups were developed. In 2015, Zhan and co-workers firstly designed and synthesized ITIC,[12] a PCE of 7% was achieved with PTB7-Th as donor polymer. Then, varied FREAs were developed and PCEs over 16% and 17% were realized in single junction and tandem OSCs, respectively.[13–15]

High efficiency FREAs normally possess planar backbones to facilitate the intramolecular charge transfer between the donor unit and the acceptor unit, and the protruded side chains to suppress self-aggregation to form large aggregates. Typically, NFAs based on indacenodithiophene (IDT) unit exhibit excellent photovoltaic performance. For examples, A–D–A type NFAs such as IDIC, IEIC, IEICO, ITOIC and IDTBOC6 consisted of a IDT core unit and two 1,1-dicyanomethylene-3-indanone electron withdrawing end groups.[16–20] As one of state-of-the-art NFAs, IDIC with planar chemical structure displays wide absorption in the range of 500–800 nm and high electron transport mobility of 1.1×10^{-3} cm^2 V^{-1} s^{-1}, which is close to fullerene derivatives and ensures effective charge carrier transport. The as-cast PSCs based on PDBT-T1:IDIC blended films showed a PCE of 8.71% and an optimal PCE of over 11% by matching with polymer donor PTFBDT-BZS.[21] IDIC was also used to fabricate OSCs with a thick active layer by Zhang *et al.*[22,23] To further extend the chemical structures, as shown in Fig. 1, NDIC was prepared by replacing the central aryl benzene unit of IDIC to a naphthalene ring, which provide a good project to explore the effect of tiny chemical structure modification on molecular energy level, absorption, and photovoltaic performance. Our result demonstrates that NDIC displays a larger optical band gap of 1.72 eV and higher lowest unoccupied molecular orbital (LUMO) energy level compared with IDIC. It is worth noting that the same acceptor was also reported by Zhan *et al.*,[24] PTB7-Th:IHIC-N based binary devices exhibited an

[a]*Key Laboratory of Eco-functional Polymer Materials of the Ministry of Education, Key Laboratory of Eco-environmental Polymer Materials of Gansu Province, College of Chemistry and Chemical Engineering, Northwest Normal University, Lanzhou 730070, China*

[b]*Beijing Key Laboratory of Energy Conversion and Storage Materials, College of Chemistry, Beijing Normal University, Beijing 100875, China. E-mail: lyh1991a@163.com; zsbo@bnu.edu.cn*

† Electronic supplementary information (ESI) available. See DOI: 10.1039/c9ra08092a

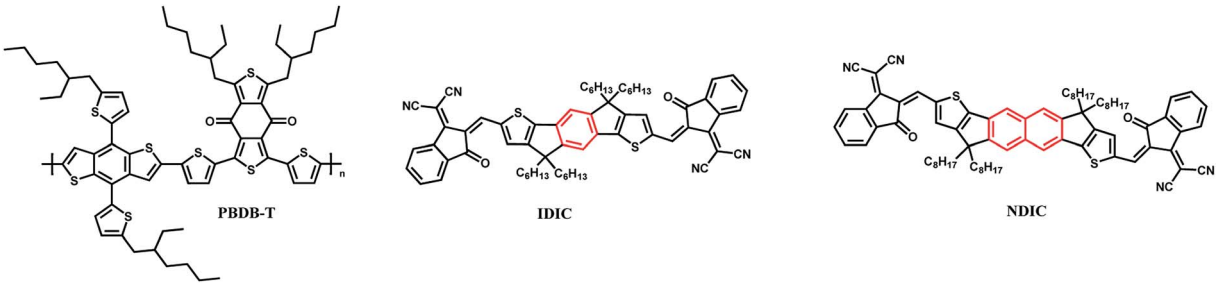

Fig. 1 Chemical structures of IDIC, NDIC and PBDB-T.

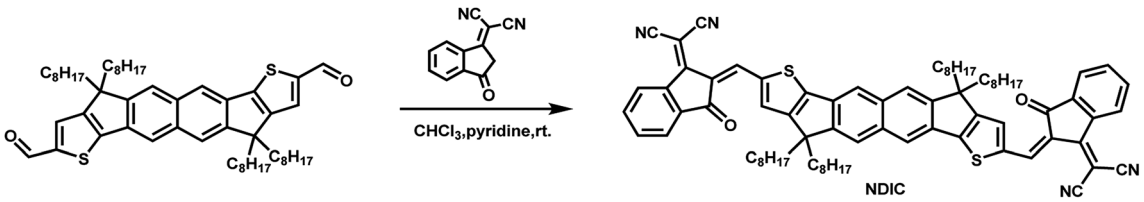

Scheme 1 The synthetic route of NDIC.

inferior PCE of 6.91% compared with its analogue IHIC (10.6%), and the ternary devices gave an improved PCE of 11.9%. To further explore the possibility of improving the photovoltaic performance of NDIC, PBDB-T was selected as the donor material due to its high hole mobility and deep HOMO energy level.[19,25–29] According to the literature, the elevated LUMO levels of acceptors and the decreased highest occupied molecular orbital (HOMO) level of donors could effectively increase the open-circuit voltage of PSCs.[30,31] Due to the elevated LUMO energy levels of NDIC, PSCs based on NDIC exhibit an V_{oc} of 0.90 V which is much higher that of IDIC (0.79 V). An optimal PCE of 9.43% was obtained for NDIC based devices.

2. Results and discussion

2.1 Material synthesis and characterization

A brief synthetic route of NDIC is shown in Scheme 1. NDIC was synthesized in a yield of 74% by Knoevenagel condensation of the dialdehyde intermediate and 2-(3-oxo-2,3-dihydro-1*H*-inden-1-ylidene)malononitrile. The detailed synthetic procedures are described in the ESI.† NDIC displays an excellent solubility in common organic solvents such as dichloromethane, chloroform and *o*-dichlorobenzene (*o*-DCB).

The packing of acceptors in films is studied by wide angle X-ray diffraction (XRD). As shown in Fig. S4,† the two acceptors display varied packing styles. IDIC exhibited a peak located at an angle of $2\theta = 24.75°$ corresponding to a π–π stacking distance of 3.59 Å. As for NDIC, a strong and sharp peak at $2\theta = 5.28°$ and a weak peak at $2\theta = 24.87°$ are observed, which correspond to a lamellar distance of 16.73 Å and a π–π stacking distance of 3.57 Å, respectively. The above results indicate that a small structural difference can cause a dramatic change in their XRD results.

2.2 Optical and electrochemical properties

Ultraviolet-visible (UV-vis) absorption spectra of NDIC and IDIC in dilute chloroform solutions and as thin films are shown in Fig. 2. In dilute chloroform solutions, NDIC displays a wide

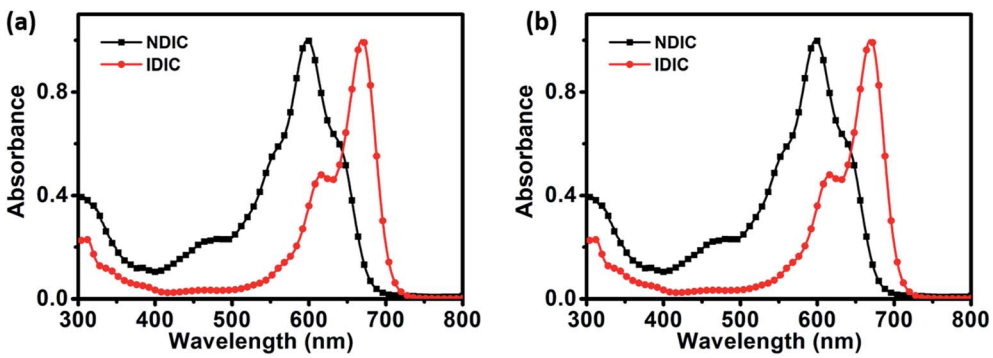

Fig. 2 Absorption spectra of NDIC and IDIC in dilute chloroform solutions (a) and as thin films (b).

Table 1 Electronic and optical properties of NDIC and IDIC

Molecules	λ_{max}^{sol} [nm]	λ_{onset}^{sol} [nm]	λ_{max}^{film} [nm]	λ_{onset}^{film} [nm]	$E_g^{opt a}$ [eV]	HOMO^b [eV]	LUMO^b [eV]
NDIC	598	690	614	734	1.72	−5.71	−3.88
IDIC	669	723	716	776	1.60	−5.69	−3.92

^{a} Estimated from the absorption edge of film ($E_g^{opt} = 1240/\lambda_{onset}$). ^{b} Energy levels evaluated by CV.

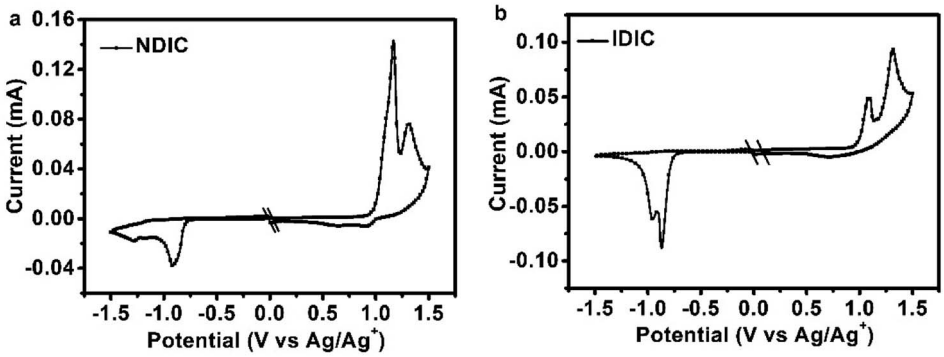

Fig. 3 Cyclic voltammetry curves of NDIC and IDIC as thin films on Pt electrode measured in 0.1 M Bu_4NPF_6 acetonitrile solutions at a scan rate of 100 mV s^{-1}.

absorption in the range of 500 to 680 nm and IDIC shows a red-shifted absorption in the range of 550 to 720 nm. The main absorption peak of NDIC and IDIC in chloroform solutions is located at 601 and 670 nm, respectively. In going from solutions to films, the absorption of both NDIC and IDIC exhibits an obvious red-shift with the maximum absorption peak located at 614 and 717 nm, respectively. The optical bandgap of NDIC is calculated to be 1.72 eV according to the equation: $E_g^{opt} = 1240/\lambda_{onset}$, which is slightly larger than that of IDIC (1.60 eV). The related optical data are also summarized in Table 1.

The HOMO and LUMO energy levels of NDIC and IDIC were measured by electrochemical cyclic voltammetry (CV) with Ag/AgCl as reference electrode calibrated with ferrocene/ferrocenium (Fc/Fc^+) redox couple (4.8 eV below vacuum).[32] From the onset oxidation/reduction potentials ($E_{ox/red}$) in the CV curves (as shown in Fig. 3), the HOMO/LUMO energy levels of NDIC and IDIC were calculated to be −5.71/−3.88 eV, −5.69/−3.92 eV, respectively, according to the equations of $E_{HOMO/LUMO} = -e(E_{ox/red} - E_{Fc/Fc^+} + 4.8)$ (eV), where $E_{ox/red}$ and E_{Fc/Fc^+} are the onset oxidation/reduction potentials and redox potential of Fc/Fc^+, respectively. Compared with IDIC, NDIC exhibits a higher LUMO energy level, which is beneficial for obtaining higher V_{oc}. The detailed data are also summarized in Table 1. The energy levels of IDIC, NDIC and other materials used for fabricating photovoltaic devices are also shown in Fig. 4.

Density functional theory (DFT) calculations at B3LYP/6-31g(d) were performed to investigate the molecular geometry and energy levels of the simplified IDIC and NDIC. The molecular backbones of simplified NDIC and IDIC are planar, which is beneficial for intermolecular π–π stacking and charge transport. The theoretically calculated LUMO/HOMO energy levels are −3.69/−5.95 eV for IDIC and −3.68/−5.97 eV for NDIC, respectively. The trend of calculated energy levels is consistent with that obtained by electrochemical measurements. The absorptions of NDIC and IDIC were calculated by DFT at CAM-B3LYP(d,p) level. As shown in Fig. S6,† the calculated absorption wavelength of simplified IDIC is 494 nm, which is much higher than that of NDIC (480 nm). The trend of calculated result is consistent with UV-vis measurement. Moreover, various configuration interactions, the natural transition orbitals (NTOs) and reorganization energies are also described in ESI.†

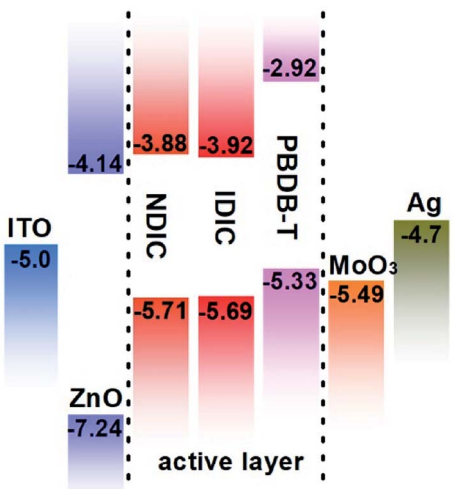

Fig. 4 Energy band diagram of NDIC and IDIC.

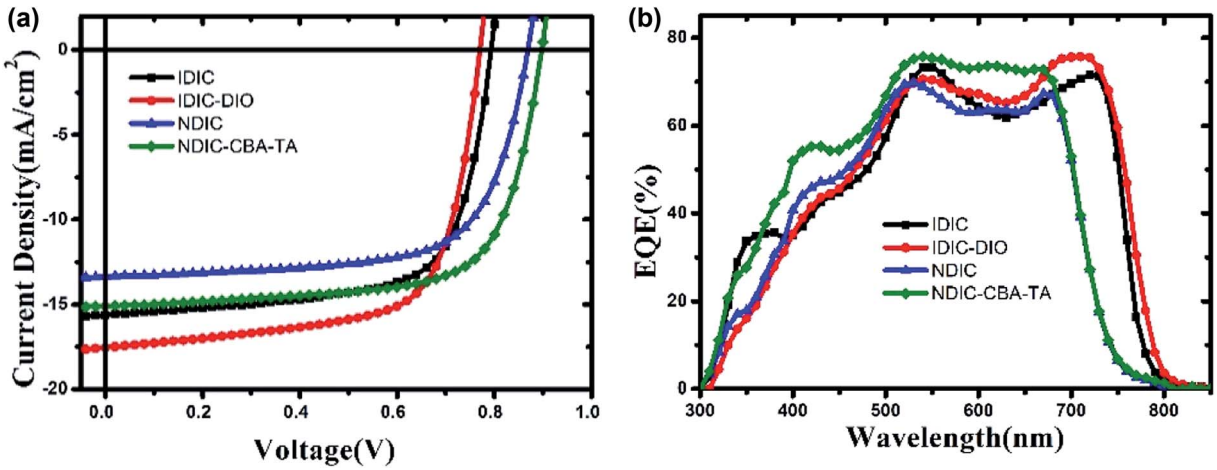

Fig. 5 (a) J–V and (b) EQE curves of NDIC and IDIC based devices.

2.3 Photovoltaic performance

The photovoltaic performance of IDIC and NDIC was investigated by fabricating inverted devices of ITO/ZnO/donor:-acceptor/MoO_3/Ag. The ZnO layer was prepared according to pervious reported procedure.[33] PBDB-T was used as the donor to evaluate the photovoltaic performance of IDIC and NDIC. A variety of conditions were optimized, such as active layer composition, spin-coating rate, additive and thermal annealing (TA) condition (Tables S2–S6†). J–V curves and EQE spectra of the optimized devices are shown in Fig. 5. The photovoltaic parameters are listed in Table 2. IDIC-based devices demonstrated a PCE of 8.47% with a V_{oc} of 0.79 V. In comparison, a PCE of 7.92% with a higher open-circuit voltage (V_{oc}) of 0.87 V was obtained for the as-cast devices based on NDIC. After a systematical optimization, the photovoltaic performance of NDIC was markedly improved, and the optimal devices gave a PCE of 9.43% with a V_{oc} of 0.90 V, a short-circuit current density (J_{sc}) of 15.10 mA cm^{-2} and a fill factor (FF) of 69.60%, which is slightly higher than that of IDIC-based devices (9.19%). Compared with NDIC and IDIC based devices, the higher V_{oc} can be attribute to the elevated LUMO energy level of NDIC.[34,35] External quantum efficiency (EQE) measurement was performed under the irradiation of monochromatic light at an interval of 10 nm. As shown in Fig. 5b, the PBDB-T:NDIC and PBDB-T:IDIC based photovoltaic devices display a wide photoelectric conversion response in the range of 300–750 nm and 300–800 nm, respectively, which is consistent with their UV-vis absorptions. The calculated J_{sc} values integrated from the EQE curves showed a 3–5% mismatch compared with those obtained from the J–V curves.

2.4 Charge mobilities

In addition, the electron and hole mobilities of IDIC and NDIC based blend films were measured by space charge-limited current (SCLC) method with device structures of ITO/ZnO/active layer/Al and ITO/PEDOT:PSS/active layer/Au, respectively. The calculated charge mobility values are listed in Table S1.† The charge mobility was calculated according to the equation: $J = 9\varepsilon_0\varepsilon_r\mu V^2/8L^3$, and the dark current $J^{1/2}$–V curves for the calculation of the electron and hole mobility are shown in Fig. S7.† For the optimal condition of PBDB-T:IDIC film, the electron and hole mobilities are 2.21×10^{-4} and 2.65×10^{-4} cm^2 V^{-1} s^{-1}, respectively; whereas for the PBDB-T:NDIC blend film prepared under optimal conditions, the electron and hole mobilities are 1.61×10^{-4} and 1.52×10^{-4} cm^2 V^{-1} s^{-1}, respectively. The PBDB-T:NDIC based devices exhibited a more balanced charge transport than PBDB-T:IDIC based ones, which could well explain the higher FF for the NDIC based devices.

2.5 Film morphology analysis

The morphology for the blend films was studied by atomic force microscope (AFM). As shown in Fig. 6b, the active layers for IDIC are homogeneous with a root-mean-square (RMS) roughness value of 1.60 nm, and more polymer fibrils with a RMS value of 2.11 nm could be observed after DIO was added. The as-cast blend film of NDIC (Fig. 6c) shows a RMS value of 2.30 nm.

Table 2 Photovoltaic parameters of NDIC and IDIC based devices

D : A	Additive	TA	V_{oc} (V)	J_{sc} (mA cm^{-2})	FF (%)	PCE (%)
PBDB-T : IDIC = 1 : 1	N/A	N/A	0.79	15.62	68.4	8.47
PBDB-T : IDIC = 1 : 1	0.3% DIO	N/A	0.77	17.54	68.0	9.19
PBDB-T : NDIC = 1 : 1.5	N/A	N/A	0.87	13.35	68.3	7.92
PBDB-T : NDIC = 1 : 1.5	0.7% CBA	140 °C	0.90	15.10	69.6	9.43

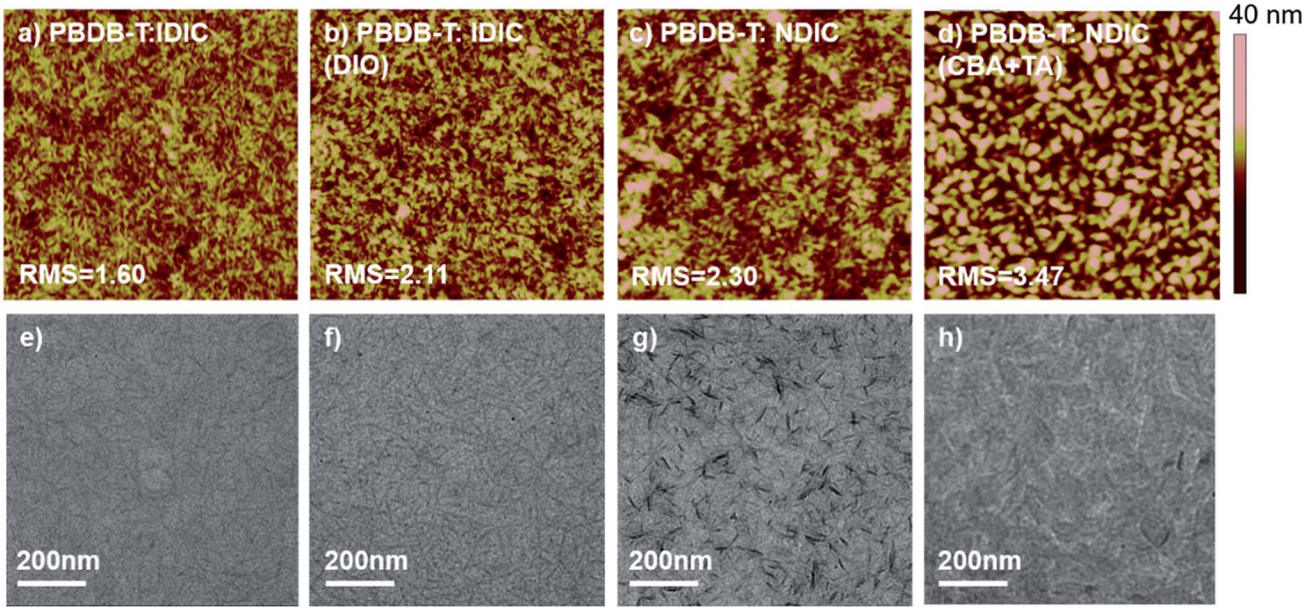

Fig. 6 AFM height images (5 × 5 μm) of the (a) PBDB-T:IDIC; (b) PBDB-T:IDIC with 0.3% DIO; (c) PBDB-T:NDIC; and (d) PBDB-T:NDIC with 0.7% CBA and 140 °C TA films and TEM images (e) PBDB-T:IDIC; (f) PBDB-T:IDIC with 0.3% DIO; (g) PBDB-T:NDIC and (h) PBDB-T:NDIC with 0.7% CBA and 140 °C TA films.

However, the addition of additive together with thermal annealing treatment, the AFM image of NDIC-based devices demonstrated a slightly rough surface with the RMS value increased to 3.47 nm. The TEM image of IDIC:PBDB-T as-cast film shows a homogeneous morphology with sparsely distributed polymer nanofibrils. After the addition of 0.3% DIO, the morphology of the blend film shows similar morphology but with more polymer nanofibrils. As for the as-cast NDIC:PBDB-T blend films, the TEM images show obvious large aggregates probably formed by the aggregation of NDIC molecules. The result is understandable and consistent with the XRD measurement. After the addition of 0.7% CBA and thermal treatment at 140 °C for 5 min, the blend film becomes more homogeneous with the dark aggregates disappeared.

3. Conclusion

In summary, an effective way was developed by tuning the energy level to achieve a high open circuit voltage. The precisely designed NFA NDIC with naphthalene as the core display an optical band gap of 1.72 eV and a LUMO level of −3.88 eV, in comparison, IDIC (benzene as the core) exhibits a narrower optical band gap of 1.60 eV and a lower LUMO level of −3.92 eV. PBDB-T was used as polymer donor to evaluate the photovoltaic performance. Solvent additives and thermal annealing were used for further device optimization. PSCs based on NDIC exhibit a high PCE of 9.43% with a V_{oc} of 0.90 V. Compared with NDIC, IDIC, a PCE of 9.19% with a lower V_{oc} of 0.77 V was achieved. These preliminary results indicate that NDIC is a promising high efficient NFA for PSCs. Our results demonstrate that the tiny variation of molecular structure could vividly affect the optical and electrochemical properties, and thus the photovoltaic performance.

Conflicts of interest

The authors declare no conflict of interest.

Acknowledgements

Financial support from the National Natural Science Foundation of China (21574013 and 51673028), the Program for Changjiang Scholars and Innovative Research Team in University is gratefully acknowledged, and China Postdoctoral Science Foundation (2018M641033).

References

1 M. Kaltenbrunner, M. S. White, E. D. Glowacki, T. Sekitani, T. Someya, N. S. Sariciftci and S. Bauer, Ultrathin and lightweight organic solar cells with high flexibility, *Nat. Commun.*, 2012, **3**, 85–100, DOI: 10.1038/ncomms1772.
2 A. J. Heeger, 25th Anniversary Article: Bulk Heterojunction Solar Cells: Understanding the Mechanism of Operation, *Adv. Mater.*, 2014, **26**, 10–28, DOI: 10.1002/adma.201304373.
3 F. C. Krebs, Processing and preparation of polymer and organic solar cells, *Sol. Energy Mater. Sol. Cells*, 2009, **93**, 393, DOI: 10.1016/j.solmat.2008.12.008.
4 S. Lizin, S. Van Passel, E. De Schepper, W. Maes, L. Lutsen, J. Manca and D. Vanderzande, Life cycle analyses of organic photovoltaics: a review, *Energy Environ. Sci.*, 2013, **6**, 3136–3149, DOI: 10.1039/c3ee42653j.

5 C. J. Brabec, Organic photovoltaics: technology and market, *Sol. Energy Mater. Sol. Cells*, 2004, **83**, 273–292, DOI: 10.1016/j.solmat.2004.02.030.

6 Y. Lin, Y. Li and X. Zhan, Small molecule semiconductors for high-efficiency organic photovoltaics, *Chem. Soc. Rev.*, 2012, **41**, 4245–4272, DOI: 10.1039/c2cs15313k.

7 W. Zhao, S. Li, H. Yao, S. Zhang, Y. Zhang, B. Yang and J. Hou, Molecular Optimization Enables over 13% Efficiency in Organic Solar Cells, *J. Am. Chem. Soc.*, 2017, **139**, 7148–7151, DOI: 10.1021/jacs.7b02677.

8 Z. Zhang, M. Li, Y. Liu, J. Zhang, S. Feng, X. Xu, J. Song and Z. Bo, Simultaneous enhancement of the molecular planarity and the solubility of non-fullerene acceptors: effect of aliphatic side-chain substitution on the photovoltaic performance, *J. Mater. Chem. A*, 2017, **5**, 7776–7783, DOI: 10.1039/c7ta02141k.

9 H. Li, J. Wang, Y. Wang, F. Bu, W. Shen, J. Liu, L. Huang, W. Wang, L. A. Belfiore and J. G. Tang, The progress of non-fullerene small molecular acceptors for high efficiency polymer solar cells, *Sol. Energy Mater. Sol. Cells*, 2019, **190**, 83–97, DOI: 10.1016/j.solmat.2018.10.016.

10 S. Dai, F. Zhao, Q. Zhang, T.-K. Lau, T. Li, K. Liu, Q. Ling, C. Wang, X. Lu, W. You and X. Zhan, Fused Nonacyclic Electron Acceptors for Efficient Polymer Solar Cells, *J. Am. Chem. Soc.*, 2017, **139**, 1336–1343, DOI: 10.1021/jacs.6b12755.

11 P. Cheng, M. Zhang, T.-K. Lau, Y. Wu, B. Jia, J. Wang, C. Yan, M. Qin, X. Lu and X. Zhan, Realizing Small Energy Loss of 0.55 eV, High Open-Circuit Voltage > 1 V and High Efficiency > 10% in Fullerene-Free Polymer Solar Cells *via* Energy Driver, *Adv. Mater.*, 2017, **29**, 1605216, DOI: 10.1002/adma.201605216.

12 Y. Lin, J. Wang, Z.-G. Zhang, H. Bai, Y. Li, D. Zhu and X. Zhan, An Electron Acceptor Challenging Fullerenes for Efficient Polymer Solar Cells, *Adv. Mater.*, 2015, **27**, 1170–1174, DOI: 10.1002/adma.201404317.

13 B. Fan, D. Zhang, M. Li, W. Zhong, Z. Zeng, L. Ying, F. Huang and Y. Cao, Achieving over 16% efficiency for single-junction organic solar cells, *Sci. China: Chem.*, 2019, **62**, 746–752, DOI: 10.1007/s11426-019-9457-5.

14 L. Meng, Y. Zhang, X. Wan, C. Li, X. Zhang, Y. Wang, X. Ke, Z. Xiao, L. Ding, R. Xia, H.-L. Yip, Y. Cao and Y. Chen, Organic and solution-processed tandem solar cells with 17.3% efficiency, *Science*, 2018, **361**, 1094–1098, DOI: 10.1126/science.aat2612.

15 L. Duan, N. K. Elumalai, Y. Zhang and A. Uddin, Progress in non-fullerene acceptor based organic solar cells, *Sol. Energy Mater. Sol. Cells*, 2019, **193**, 22–65, DOI: 10.1016/j.solmat.2018.12.033.

16 Y. Lin, Q. He, F. Zhao, L. Huo, J. Mai, X. Lu, C.-J. Su, T. Li, J. Wang, J. Zhu, Y. Sun, C. Wang and X. Zhan, A Facile Planar Fused-Ring Electron Acceptor for As-Cast Polymer Solar Cells with 8.71% Efficiency, *J. Am. Chem. Soc.*, 2016, **138**, 2973–2976, DOI: 10.1021/jacs.6b00853.

17 Y. Lin, Z. Zhang, H. Bai, J. Wang, Y. Yao, Y. Li, D. Zhu and X. Zhan, High-performance fullerene-free polymer solar cells with 6.31% efficiency, *Energy Environ. Sci.*, 2015, **8**, 610–616, DOI: 10.1039/c4ee03424d.

18 H. Yao, Y. Chen, Y. Qin, R. Yu, Y. Cui, B. Yang, S. Li, K. Zhang and J. Hou, Design and Synthesis of a Low Bandgap Small Molecule Acceptor for Efficient Polymer Solar Cells, *Adv. Mater.*, 2016, **28**, 8283–8287, DOI: 10.1002/adma.201602642.

19 Y. Liu, C. Zhang, D. Hao, Z. Zhang, L. Wu, M. Li, S. Feng, X. Xu, F. Liu, X. Chen and Z. Bo, Enhancing the Performance of Organic Solar Cells by Hierarchically Supramolecular Self-Assembly of Fused-Ring Electron Acceptors, *Chem. Mater.*, 2018, **30**, 4307–4312, DOI: 10.1021/acs.chemmater.8b01319.

20 Y. Liu, Z. Zhang, S. Feng, M. Li, L. Wu, R. Hou, X. Xu, X. Chen and Z. Bo, Exploiting Noncovalently Conformational Locking as a Design Strategy for High Performance Fused-Ring Electron Acceptor Used in Polymer Solar Cells, *J. Am. Chem. Soc.*, 2017, **139**, 3356–3359, DOI: 10.1021/jacs.7b00566.

21 Y. Lin, F. Zhao, Y. Wu, K. Chen, Y. Xia, G. Li, S. K. K. Prasad, J. Zhu, L. Huo, H. Bin, Z.-G. Zhang, X. Guo, M. Zhang, Y. Sun, F. Gao, Z. Wei, W. Ma, C. Wang, J. Hodgkiss, Z. Bo, O. Inganäs, Y. Li and X. Zhan, Mapping Polymer Donors toward High-Efficiency Fullerene Free Organic Solar Cells, *Adv. Mater.*, 2017, **29**, 1604155, DOI: 10.1002/adma.201604155.

22 Q. Fan, Y. Wang, M. Zhang, B. Wu, X. Guo, Y. Jiang, W. Li, B. Guo, C. Ye, W. Su, J. Fang, X. Ou, F. Liu, Z. Wei, T. C. Sum, T. P. Russell and Y. Li, High-Performance As-Cast Nonfullerene Polymer Solar Cells with Thicker Active Layer and Large Area Exceeding 11% Power Conversion Efficiency, *Adv. Mater.*, 2018, **30**, 1704546, DOI: 10.1002/adma.201704546.

23 B. Guo, W. Li, X. Guo, X. Meng, W. Ma, M. Zhang and Y. Li, High Efficiency Nonfullerene Polymer Solar Cells with Thick Active Layer and Large Area, *Adv. Mater.*, 2017, **29**, 1702291, DOI: 10.1002/adma.201702291.

24 J. Zhang, C. Yan, W. Wang, Y. Xiao, X. Lu, S. Barlow, T. C. Parker, X. Zhan and S. R. Marder, Panchromatic Ternary Photovoltaic Cells Using a Nonfullerene Acceptor Synthesized Using C–H Functionalization, *Chem. Mater.*, 2018, **30**, 309–313, DOI: 10.1021/acs.chemmater.7b04499.

25 Y. Cui, C. Yang, H. Yao, J. Zhu, Y. Wang, G. Jia, F. Gao and J. Hou, Efficient Semitransparent Organic Solar Cells with Tunable Color enabled by an Ultralow-Bandgap Nonfullerene Acceptor, *Adv. Mater.*, 2017, **29**, 1703080, DOI: 10.1002/adma.201703080.

26 Z. Fei, F. D. Eisner, X. Jiao, M. Azzouzi, J. A. Rohr, Y. Han, M. Shahid, A. S. R. Chesman, C. D. Easton, C. R. McNeill, T. D. Anthopoulos, J. Nelson and M. Heeney, An Alkylated Indacenodithieno[3,2-*b*]thiophene-Based Nonfullerene Acceptor with High Crystallinity Exhibiting Single Junction Solar Cell Efficiencies Greater than 13% with Low Voltage Losses, *Adv. Mater.*, 2018, **30**, 1705209, DOI: 10.1002/adma.201705209.

27 W. Jiang, R. Yu, Z. Liu, R. Peng, D. Mi, L. Hong, Q. Wei, J. Hou, Y. Kuang and Z. Ge, Ternary Nonfullerene Polymer Solar Cells with 12.16% Efficiency by Introducing One

Acceptor with Cascading Energy Level and Complementary Absorption, *Adv. Mater.*, 2018, **30**, 1703005, DOI: 10.1002/adma.201703005.

28 B. Kan, J. Zhang, F. Liu, X. Wan, C. Li, X. Ke, Y. Wang, H. Feng, Y. Zhang, G. Long, R. H. Friend, A. A. Bakulin and Y. Chen, Fine-Tuning the Energy Levels of a Nonfullerene Small-Molecule Acceptor to Achieve a High Short-Circuit Current and a Power Conversion Efficiency over 12% in Organic Solar Cells, *Adv. Mater.*, 2018, **30**, 1704904, DOI: 10.1002/adma.201704904.

29 W. Zhao, D. Qian, S. Zhang, S. Li, O. Inganas, F. Gao and J. Hou, Fullerene-Free Polymer Solar Cells with over 11% Efficiency and Excellent Thermal Stability, *Adv. Mater.*, 2016, **28**, 4734–4739, DOI: 10.1002/adma.201600281.

30 L. Yuan, K. Lu, B. Xia, J. Zhang, Z. Wang, Z. Wang, D. Deng, J. Fang, L. Zhu and Z. Wei, Acceptor End-Capped Oligomeric Conjugated Molecules with Broadened Absorption and Enhanced Extinction Coefficients for High-Efficiency Organic Solar Cells, *Adv. Mater.*, 2016, **28**, 5980–5985, DOI: 10.1002/adma.201600512.

31 J.-L. Wang, Z. Wu, J.-S. Miao, K.-K. Liu, Z.-F. Chang, R.-B. Zhang, H.-B. Wu and Y. Cao, Solution-Processed Diketopyrrolopyrrole-Containing Small-Molecule Organic Solar Cells with 7.0% Efficiency: In-Depth Investigation on the Effects of Structure Modification and Solvent Vapor Annealing, *Chem. Mater.*, 2015, **27**, 4338–4348, DOI: 10.1021/acs.chemmater.5b00848.

32 Q. Sun, H. Wang, C. Yang and Y. Li, Synthesis and electroluminescence of novel copolymers containing crown ether spacers, *J. Mater. Chem.*, 2003, **13**, 800–806, DOI: 10.1039/b209469j.

33 Y. Sun, J. H. Seo, C. J. Takacs, J. Seifter and A. J. Heeger, Inverted Polymer Solar Cells Integrated with a Low-Temperature-Annealed Sol-Gel-Derived ZnO Film as an Electron Transport Layer, *Adv. Mater.*, 2011, **23**, 1679–1683, DOI: 10.1002/adma.201004301.

34 E. Jin, C. Du, M. Wang, W. Li, C. Li, H. Wei and Z. Bo, Dibenzothiophene-Based Planar Conjugated Polymers for High Efficiency Polymer Solar Cells, *Macromolecules*, 2012, **45**, 7843–7854, DOI: 10.1021/ma301622g.

35 B. P. Rand, D. P. Burk and S. R. Forrest, Offset energies at organic semiconductor heterojunctions and their influence on the open-circuit voltage of thin-film solar cells, *Phys. Rev. B: Condens. Matter Mater. Phys.*, 2007, **75**, 115327, DOI: 10.1103/PhysRevB.75.115327.